

Lifted Turbulent Premixed Flames Issuing Into a Hot Coflow, Imaging of Temperature and OH

Matthew J. Dunn*, Assaad R. Masri and Robert W. Bilger

School of Aerospace, Mechanical and Mechatronic Engineering, The University of Sydney, N.S.W. 2006, Australia

Abstract

The experimental results of simultaneous 2D laser Rayleigh scattering and OH Planar Laser Induced Fluorescence (PLIF) imaging applied to lifted turbulent premixed flames issuing into a hot coflow are reported. Jet mixtures of methane-air with equivalence ratios 0.5 and 0.6 with corresponding hot coflow temperatures of 1500K and 1650K respectively are studied. The impact on flame structure of increasing the jet Reynolds number for a constant equivalence ratio is examined. The instantaneous structure of these flames is presented and described qualitatively; quantitative comparison of the flames is examined using temperature, temperature gradient and OH mole fraction results. For the high velocity flames OH concentrations are found to be lower than the hot coflow upstream from the main flame base; indicating that the lifted premixed flame stabilization process may be limited by a finite-rate chemistry process.

Introduction

In previous publications [1,4] the piloted premixed jet burner (PPJB) has been shown to be a useful experimental tool to investigate highly turbulent premixed combustion. The PPJB is able to stabilise highly turbulent flames with $u'/S_L \gg 20$ due to the shrouding effect of the hot coflow, preventing dilution and reaction quenching effects. In order to achieve initial ignition in the PPJB a stoichiometric pilot is utilised, which is at a different equivalence ratio to the central jet and the hot coflow. Laser diagnostics applied to the PPJB have shown that extinction and re-ignition characteristics are possible in premixed combustion. Diagnostics results have also shown [4] that an increased thickening of the instantaneous temperature flame front with increased turbulence intensity occurs in the PPJB, correlating with the trends reported in Chen *et al.* [8].

Although the pilot is necessary to enable extinction and re-ignition behaviour in the PPJB, it adds an additional level of complication to the problem by adding a second composition stream. This added composition stream makes the numerical prediction of the PPJB difficult for some numerical models developed for premixed combustion. By removing the stoichiometric pilot from the PPJB, it is possible to characterize the burner boundary conditions with a single temperature based reaction progress variable c_T . This assumes that the coflow temperature is set to the same temperature as the adiabatic flame temperature of the central jet reactants. This configuration of the PPJB is examined in this paper and is referred to as the "premixed jet burner" (PJB).

Wu *et al.* [9] and Chen *et al.* [8] have investigated the structure of premixed flames in a Bunsen burner geometry that have a small pilot and are also referred to as "premixed jet burners". Such flows are somewhat different from those discussed here since the main jet may interact with the hot coflow at any axial location. In both [9,8] the reported flame brush structure is essentially an elongated form of the "piloted Bunsen" geometry, with the mean flame brush initially

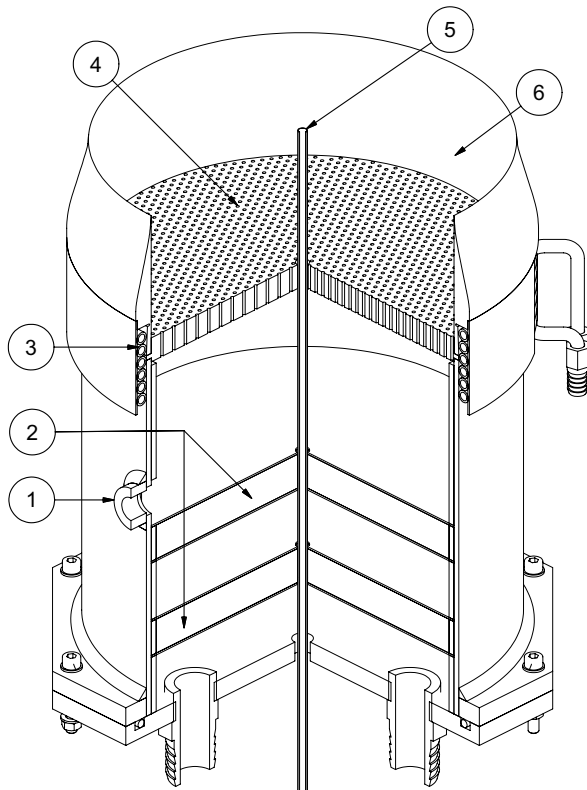
anchored close to the exit of the central jet. The flames produced in the PJB all can be described as having a mean flame brush occurring well downstream from the central jet exit, being possibly described as a "lifted premixed jet flame". Due to the lifted nature of the mean flame brush in the PJB the classification of being in the "piloted jet burner" maybe limiting, as finite-rate chemistry effects are not prominent in [9,8], where as due to the PJB flames being lifted in nature an ignition delay or initial extinction process must occur indicating finite-rate chemistry effects being a crucial factor to the flame stabilisation process.

As an addition to examining premixed combustion in a new geometrical configuration, it is possible that further understanding can be gained from the PJB in the controversial area of lifted non-premixed and partially premixed flame stabilization mechanism. Under different conditions it has been argued that lifted flame stabilisation can be due to either triple, premixed or auto-igniting flame propagation. Whilst in no way solving the lifted flame controversy the PJB can help to understand the stabilisation mechanisms in a pure premixed environment where premixed or auto-ignition is the flame stabilisation mechanism. It should be emphasised that since the fuel is premixed here then mixing of the two streams is not necessary for a flame to be stabilised.

Burner Setup and Characteristics

The PJB shown in schematic form in Figure 1, is very similar to the PPJB used in previous investigations; however as previously mentioned the PJB does not have a pilot, essentially making the geometry identical to the burner geometry used for non-premixed combustion investigations in auto-ignition studies [10]. The central jet of the PPJB is a smooth bored stainless steel tube with a 4.0 mm inside diameter (ID) and a 4.5 mm outside diameter (OD), protruding 70mm from the coflow base plate. The hot coflow is produced from the combustion products of a premixed hydrogen-air flame anchored on a 198 mm OD perforated brass disk, with $\sim 2000 \times 1.6$ mm diameter holes. Surrounding the hot coflow is a streamlined collar and a 0.8 m/s filtered air co-flowing wind tunnel to maximise the length of the hot coflow potential core. With these measures it is shown in Dunn [4], that the central jet combustion process is shielded from ambient cold air entrainment at $x/D=60$ up to a normalised radius of $r/D=4$.

Six flames in the PJB are initially identified for further study. The six flame conditions are summarised in Table 1, noting that the NPM1 and NPM2 flames have coflow temperatures equal to the adiabatic flame temperature of the central jet reactants, whilst for the NPM4 flames the coflow temperature is lower than the central jet composition adiabatic flame temperature. The flame selection for the PJB is based on selecting a single central jet composition and finding two central jet velocities that produce a medium lift off and a high lift off flame. Example mean chemiluminescence images of the low velocity NPM2-40 flame and the high velocity



Balloon number	Description
1	Flashback over-pressure sensing port
2	Glass bead filled cavities
3	Cooling water coil
4	Coflow perforated baseplate
5	Central jet exit
6	Coflow collar

Figure 1. Cross sectional view of the PJB, with all major features labelled.

Flame Code	Φ_{CJ}	U_0 (m/s)	Re	T_c (K)
NPM1-10	0.50	10	2500	1500
NPM1-40	0.50	40	10000	1500
NPM2-40	0.60	40	10000	1650
NPM2-200	0.60	200	50000	1650
NPM4-30	0.80	30	7500	1500
NPM4-100	0.80	100	25000	1500

Table 1. Summary of the flame conditions used for the experiments presented.

Φ	T_{ad} (K)	S_L (m/s)	δ_{th} (mm)	t_f (ms)
0.50	1490	0.061	1.7	28
0.60	1660	0.12	0.99	8.3
0.80	2000	0.28	0.54	1.9

Table 2. Freely propagating laminar premixed flame characteristics for the three central jet CNG-air compositions used for the experimental results presented. δ_{th} is taken to be the laminar flame thermal thickness based on the maximum gradient. t_f is defined as the laminar flame thermal time scale (δ_{th}/S_L).

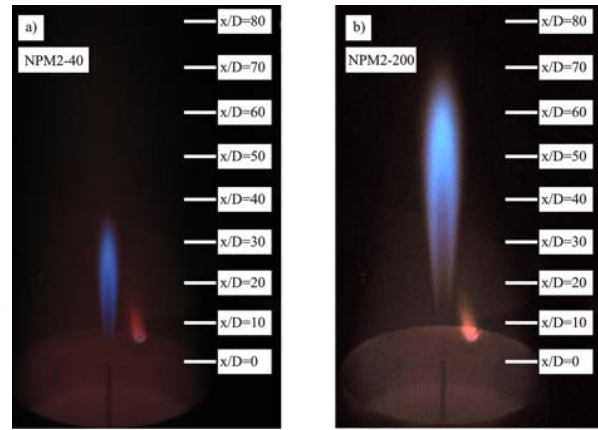


Figure 2. Mean flame luminosity images of the NPM2-40 a), and NPM2-200 b) flames. The small red region to the right of the central jet is the coflow pilot, this pilot flame in way influences the central jet combustion process

NPM2-200 flame are presented in figure 2a and 2b. Although the NPM1 and NPM4 mean chemiluminescence images are not shown, the flame characteristics and appearance are very similar to the NPM2 flames presented in figure 2. The freely propagating laminar premixed flame parameters for the three central jet compositions are presented in Table 2. These results were computed with GRI 3.0 [11] and multi-component diffusion using the open source code Cantera [5].

Laser Diagnostics Setup

In order to investigate the instantaneous temperature and local radical pool concentrations, simultaneous Rayleigh scattering and OH Laser Induced Fluorescence (LIF) has been conducted. An overview of the entire laser diagnostic experimental setup is given in figure 3. The Rayleigh scattering signal is generated by the frequency doubled output of a Q-switched Nd:YAG laser (Spectra Physics Pro 350) at 532nm, yielding 1.33 J at the probe volume. The Rayleigh beam is focused by a 300mm focal length fused silica lens into a sheet 13mm high. The laser sheet thickness of the Rayleigh beam is measured by rotating the final cylindrical lens by 90 degrees and subsequently imaging the flat beam via Rayleigh scattering. By fitting a Gaussian function to the resultant beam profile at the focal point results in a full width half maximum (FWHM) measurement of the beam thickness of $80 \pm 12 \mu\text{m}$.

The OH LIF is generated by the frequency doubled output of a pulsed Nd:YAG laser (Spectra Physics Pro 350) pumping a Syrah dye laser using Rhodamine 6G in ethanol. The fundamental of the dye laser is subsequently doubled to produce an Ultra Violet (UV) laser beam at 283.01nm for $A^2\Sigma^+ - X^2\Pi(1,0)$ excitation of OH, predominately pumping the $Q_1(6)$ line. The UV energy at the probe volume is measured to be 11mJ, at a FWHM line width of 0.15cm^{-1} obtained by deconvolution of a spectral scan over the spectrally isolated $P_1(1)$ line. The UV beam is expanded and passed through a spatial modulator to improve beam quality, with the focal length being adjusted so as to make the beam waist at the probe volume coincide with the 532nm beam waist. The UV beam is formed into a sheet 12mm in height with an $80\mu\text{m}$ FWHM sheet thickness at the waist. The UV beam waist is measured by again rotating the final cylindrical lens and imaging the LIF produced from acetone vapour.

The 532nm Rayleigh scattering signal is collected at 90° by a modified Komura 85mm $f_{\#}1.4$ lens, imaging the Rayleigh

signal directly onto a Charge Coupled Device camera at a magnification of 0.20. The inter-line transfer CCD camera for the Rayleigh signal collection (LaVision FlowMaster 3S) has 1280 x 1024 pixels with individual pixel sizes of 6.7 μm x 6.7 μm and a quantum efficiency of 36% at 532nm. Flame luminosity and OH LIF signal are totally suppressed from the Rayleigh camera by a 532nm 10nm FWHM interference filter combined with a 500ns camera gate time. On chip binning of 2x2 is selected to be the best compromise between spatial resolution and signal to noise ratio (SNR). This gives an effective probe volume to projected super-pixel pixel size of 34 μm . The single shot SNR of the Rayleigh imaging system prior to image smoothing is found to be 40, measured in a uniform field of 298K filtered air.

The Rayleigh imaging system Step Response Function (SRF) is measured using the scanning knife edge method outlined by Wang *et al.* [7] and references contained within. From the SRF the Line Spread Function (LSF) is calculated and a FWHM of 40 μm is predicted. Utilising the analysis of Wang *et al.* [7] with the computed LSF resolution, dissipation structures with measured widths greater than 134 μm an error contribution of less than 10% on the peak measured dissipation value can be attributed due to the finite spatial resolution of the imaging system.

The OH LIF collection system is based on a lens coupled intensified CCD system. Flame luminosity, 532nm and 283nm Rayleigh scattering is reject completely by two 2mm thick UG11 and a single 2mm thick WG305 Schott coloured glass filters combined with a 2 μs gate time. A 105mm $f_{\#}4.5$ Nikkor UV lens is coupled to an 18mm 2nd generation UV sensitive intensifier and subsequently lens coupled by two Nikkor 50mm $f_{\#}1.2$ lenses to a CCD camera. The LSF for the OH collection system is found to be 127 μm FWHM, this value of the LSF is much larger than the Rayleigh system due to the inclusion of the intensifier.

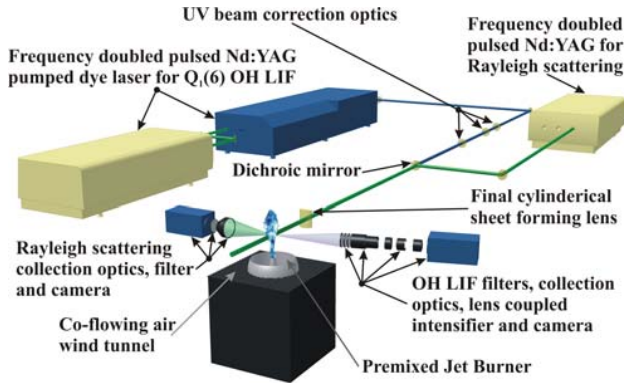


Figure 3. Experimental schematic showing lasers, laser beam paths, laser and collection optics, imaging collection system and the PJB

Data Reduction

To determine the sensitivity of the Rayleigh cross section and OH quenching rate to composition and temperature variations, laminar flame simulations are conducted for freely propagating, opposed flow and mixing limit using the Cantera code [5]. It is found to be advantageous in terms of data processing to cast the Rayleigh cross section and quenching rate dependencies with respect to the normalised Rayleigh signal as opposed to temperature. A maximum error of 2% is predicted for the Rayleigh cross section based on these calculations; however as can be seen from figure 4 the average error in cross section over the entire temperature range is

smaller than this. The Rayleigh images were converted to temperature assuming an ideal gas and corrected for background reflections and normalised using the scheme developed in Dunn *et al.* [3]. Although the Rayleigh cross section error the actual temperature measurement uncertainty is larger than 2% particularly at high temperatures, a preliminary estimate if the temperature uncertainty at 1600K is 6% considering effects such as readout noise, shot noise, errors in beam sheet correction and cross section error.

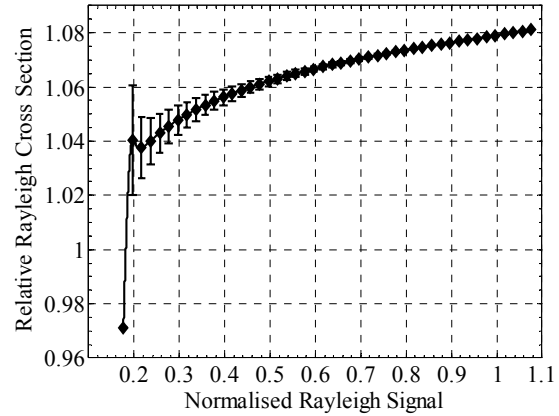


Figure 4. Numerical simulation results for the Rayleigh cross section variation vs. normalised Rayleigh signal. The normalised Rayleigh signal is taken to be the numerically calculated Rayleigh signal divided by the corresponding Rayleigh signal of ambient air. The error bars show the bounds for low strain and high strain rate simulations.

The OH LIF quenching rate variation with temperature and composition follows a similar trend for data spread and uncertainty than the Rayleigh cross section does, with a maximum error of 2%. The OH electronic and vibrational energy transfer rates and calculation method were taken from Dunn *et al.* [4] and references contained within. Due to the low OH mole fractions that occur in lean premixed combustion the OH LIF SNR can typically be very low if linear LIF techniques are employed and laser sheet thickness less than 250 μm . To obtain an acceptable SNR for the OH LIF we have employed non-linear OH LIF and further developed the quantification method presented in Dunn *et al.* [3]. Using this quantification method the collected fluorescence F can be expressed as:

$$F = \eta n_{\text{OH}} \frac{4\tau_1 \Delta z \Delta t}{\tau_2} \left[\tau_2 + \frac{\tau_3}{I_L^0} \text{dil} \log \left(\frac{\tau_3 + I_L^0 \tau_2}{\tau_3} \right) \right] \quad (1)$$

The simplifying parameters in Eq.1 τ_1 , τ_2 , and τ_3 involve Einstein coefficients, Boltzmann fraction, and temperature dependant electronic and vibrational transfer rates. The Einstein A_{ji} , B_{ji} and B_{ij} coefficient values necessary for Eq.1 were taken from LIFBASE [6]. Determination of the optical system efficiency η is determined from a calibration in the post flame gasses of a premixed flat flame burner.

Results

Mean radial profiles for the NPM2-40 and NPM2-200 flames are presented in figures 5 and 6. The NPM2-40 flame in figure 2a indicates that the mean flame base initially occurs close to $r/D=5$; figure 5 as well as figure 9a show that there is a small increase in the mean OH above the equilibrium levels of OH occurring in the coflow, this indicates that the flame is undergoing a low level of reaction at $x/D=5$. Further

downstream at $x/D=15$ it is evident from figure 7b that a reaction zone is present due to the elevated levels of OH, close to the levels found in laminar opposed flow simulations. At $x/D=25$ from figure 5 the mean temperature profile is close to equilibrium and that super equilibrium levels of OH occur in post flame oxidation zone where slow oxidation reactions limit the rate at which OH is reduced to thermal equilibrium levels. The mean flame luminosity images indicate that the mean flame brush is conical in shape, similar to an elongated Bunsen shape tapering to a tip around $x/D=20-25$. This description ties in well with the results for the mean temperature and OH profiles in figure 5, with the mean temperature profile at $x/D=25$ indicating a closed mean flame brush.

For the NPM2-200 there is no indication that any reaction at all is occurring at $x/D=5$, as the mean OH radial profile at this location does not increase above the coflow levels. Instantaneous images of OH at this location backup this finding as only ~4% of the realizations from the large data set could small regions of OH level just above the coflow level be found. The instantaneous realisation presented in figure 10a is a representative example of an image in which no OH can be above the coflow levels. Even the few images where regions of OH above the coflow level can be found, the OH magnitude is so small that it is indiscernible using the color map employed in figure 10. At $x/D=25$ it is evident from both figure 2b and figure 6 that the mean flame brush walls have not merged like they have at this axial location for the NPM2-40 flame. Figure 10 reveals that the instantaneous flame front undergoes a significant degree of mixing and thickening to the point where large regions of partially reacted gas are present.

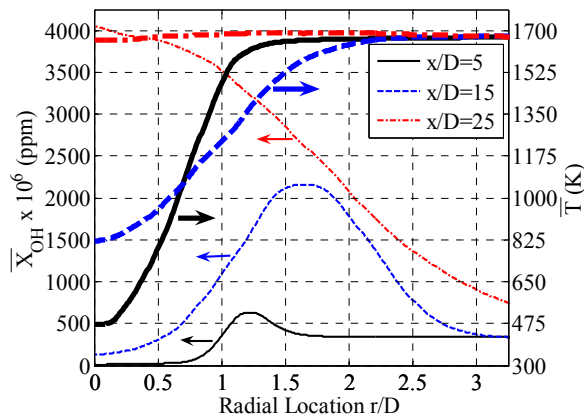


Figure 5. Radial Profiles of the Reynolds mean OH and temperature at $x/D=5, 15$ and 25 for the NPM2-40 flame.

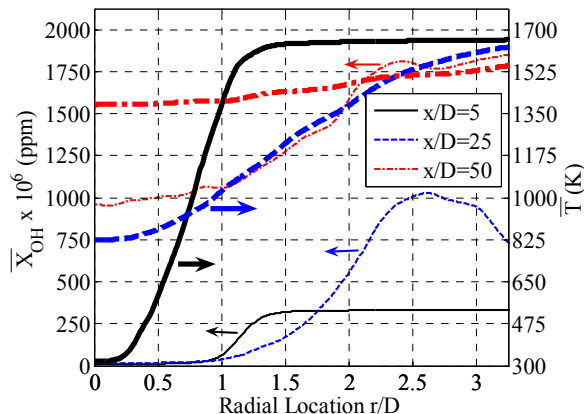


Figure 6. Radial Profiles of the Reynolds mean OH and temperature at $x/D=5, 25$ and 50 for the NPM2-200 flame.

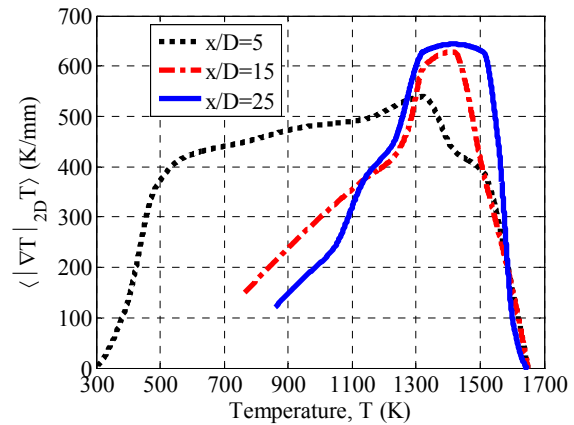


Figure 7. Comparison of the ensemble Reynolds mean 2D temperature gradient conditional on temperature for the NPM2-40 flame computed from images at $x/D=5, 15$ and 25 .

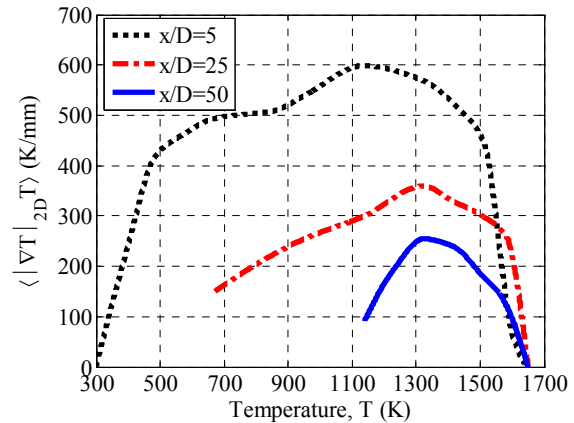


Figure 8. Comparison of the ensemble Reynolds mean 2D temperature gradient conditional on temperature for the NPM2-200 flame computed from images at $x/D=5, 25$ and 50 .

The flame structure for the NPM2 is quite unlike what would be expected from the results of a strained laminar premixed flamelets where straining compresses the instantaneous flame front reducing the instantaneous flame front thickness. From the results shown for NPM2-200 flame the flame conditions are not consistent with laminar flamelets. This is based on the observation that the high central jet velocity in the NPM2-200 produces very high turbulence intensities such that both NPM2 flames would fall into what is classified as the “Distributed Reaction Zone Regime”.

Statistically validating the idea of increased thickening of the instantaneous flame front beyond the single realisations presented in figures 9 and 10 are the plots of mean 2D temperature gradients conditional on temperature as presented in figures 7 and 8. The simulated unstrained laminar premixed gradient peaks at close to 1400 K/mm at 1200K, both the NPM2 flames have mean temperature gradients that are well below this value, by at least by a factor of 2. Due to the nature of the geometry and previous investigations of free jets into a hot coflow [4] it is reasonable to expect that the jet turbulence intensity will decay with axial location. From figure 7 the increase in the mean temperature gradient with axial location at $x/D=15$ and 25 from the value at $x/D=5$ can possibly be attributed to the decrease in turbulence intensity with axial location allowing less interaction and embedding of turbulence in the flame front and flame reaction to progress at a rate closer to the laminar value. This explanation, it would seem, is

contradicted by the results for the NPM2-200 in figure 8, here the conditional mean temperature gradient decreases with increasing axial location. It is proposed that the continued decrease in conditional mean temperature gradient is due to the inherently high turbulence intensities in the NPM2-200 flame that persist to continue finite rate chemistry effects well

down stream. As an addition, the chemical time scale will also increase as a function of downstream location due to entrainment and dilution with hot combustion products.

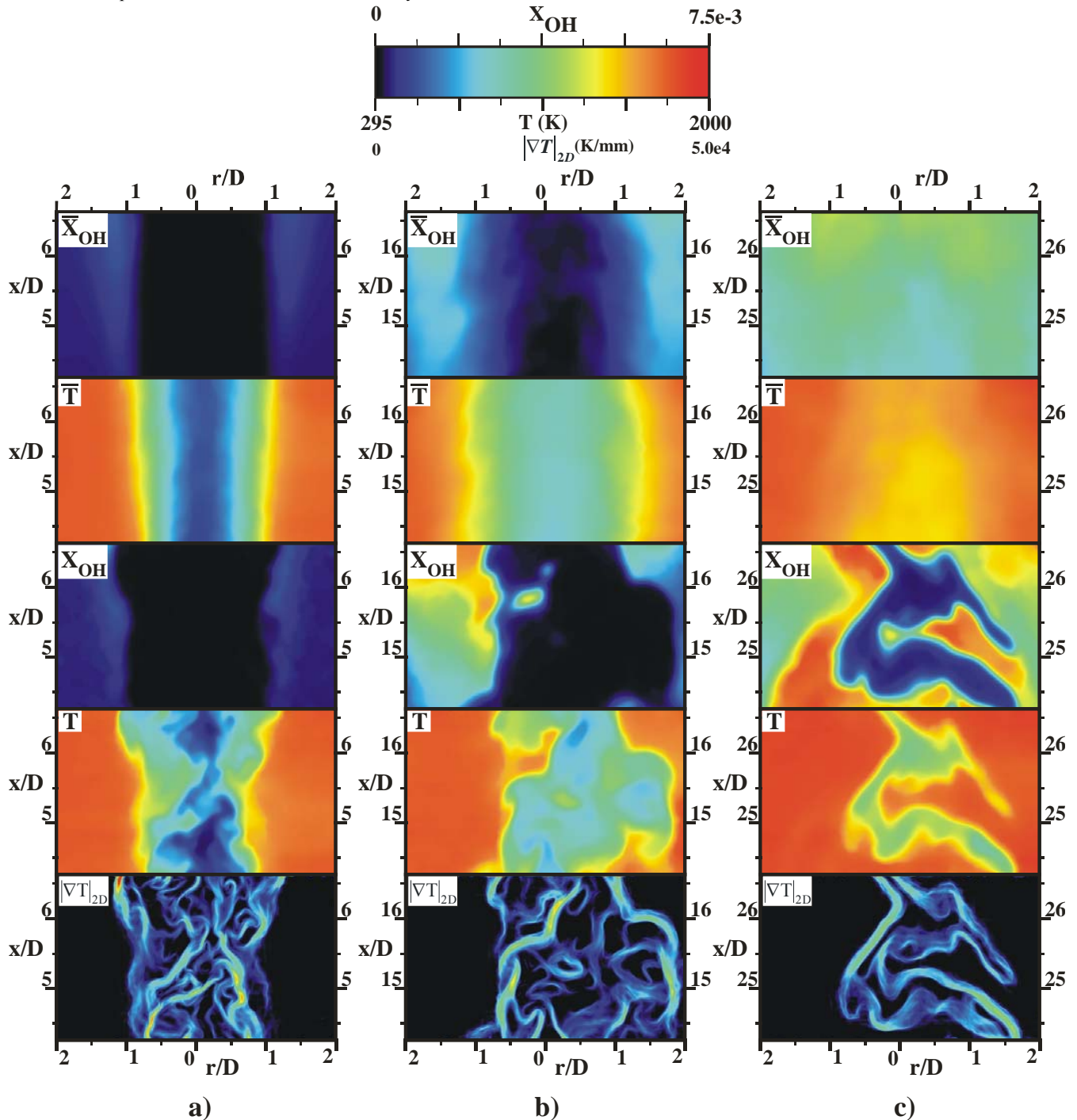


Figure 9. Mean Temperature and OH images combined with a representative instantaneous realisation of temperature, OH and the computed temperature gradient for the NPM2-40 flame a) centred at $x/D=5$, b) $x/D=15$ and c) $x/D=25$

Conclusions

The initial flame identification and characterisation combined with simultaneous Rayleigh OH-LIF imaging results are presented here for a premixed flame issuing into a hot coflow. The flames identified for further study form a stable flame brush sufficiently far downstream from the central jet exit plane to label them a lifted premixed flame. The lifted premixed flames in the

PJB are not readily characterised by any of the categories currently used for benchmark premixed flame validation, thus it is suggested a new category of premixed “lifted premixed flames” be introduced to categorise the flames produced by the PJB. In summary the PPJB is a useful experimental tool to investigate highly turbulent premixed combustion in a hot coflow resulting in a lifted premixed flame. Experimental results from

the PJB will be useful in validating turbulent premixed model validity under highly turbulent conditions and undergoing finite-rate chemistry effects. Future work will focus on further

quantitative analysis and comparison of the imaging data that has been partially presented in this paper.

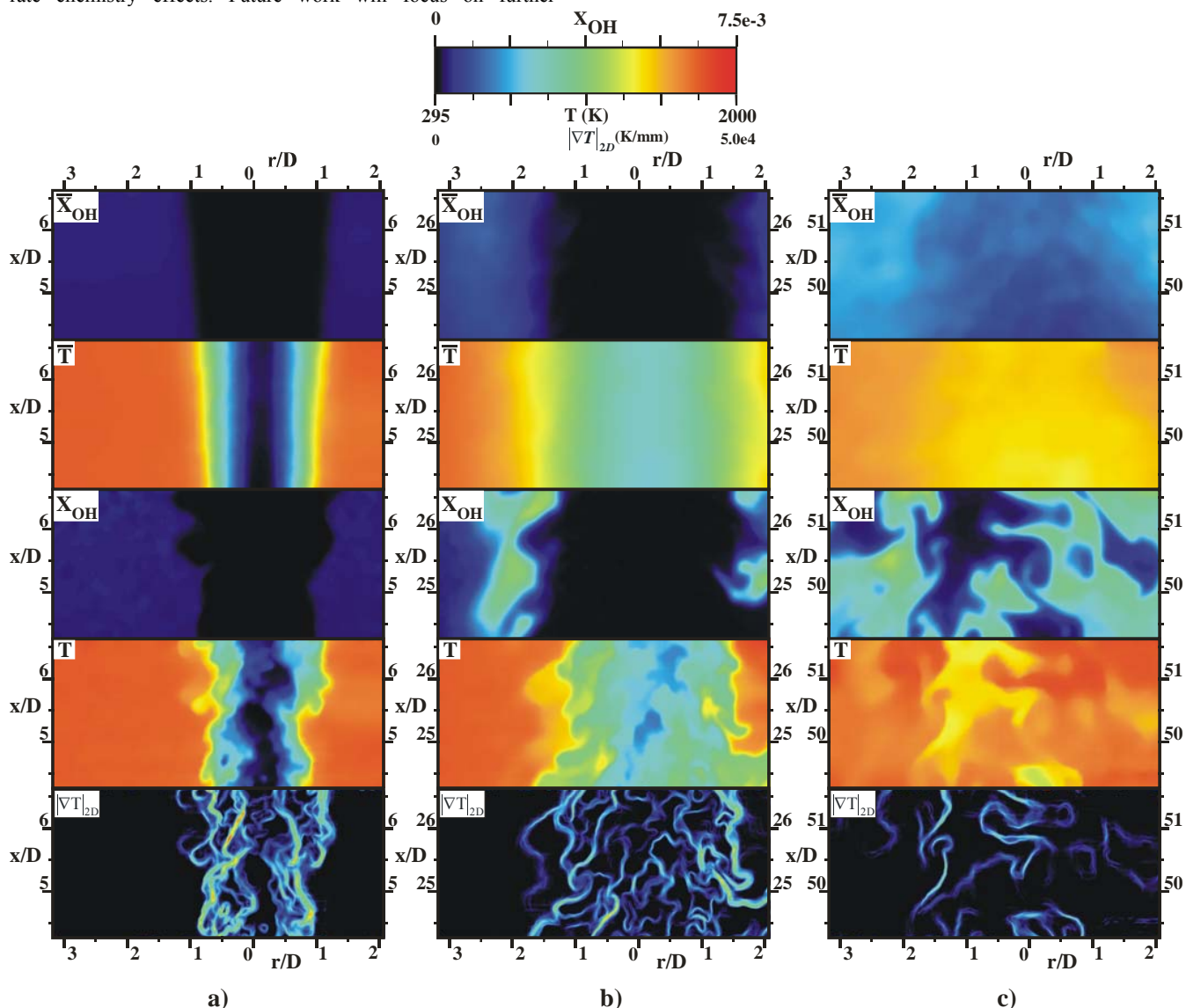


Figure 10. Mean Temperature and OH images combined with a representative instantaneous realisation of temperature, OH and the computed temperature gradient for the NPM2-200 flame a) centred at $x/D=5$ a), $x/D=25$ b) and $x/D=50$ c).

Acknowledgments

This work was supported by the Australian Research Council.

References

- [1] Bilger, R.W., Pope, S.B., Bray, K.N.C. and Driscoll, J.F., Paradigms in turbulent combustion research, *Proceedings of the Combustion Institute*. 30 (2004) 21-42.
- [2] Dunn, M.J., Bilger, R.W. and Masri, A.R., in *Proceedings of The Fifth Asia-Pacific Conference on Combustion*, 417-420, The University of Adelaide, (2005).
- [3] Dunn, M.J., Masri, A.R. and Bilger, R.W., in *Proceedings of The Fourth Australian Conference on Laser Diagnostics in Fluid Mechanics and Combustion*, 417-420, The University of Adelaide, (2005).
- [4] Dunn, M.J., Masri, A.R. and Bilger, R.W., A new Piloted Premixed Jet Burner to study strong finite-rate chemistry effects, *Combustion and Flame*. 151 (2007) 46-60.
- [5] Goodwin, D.G., in *Proceedings CVD XVI and EuroCVD Fourteenth*, Ed M. Allendorf (2003).
- [6] Luque, J. and Crosley, D.R., LIFBASE: Database and Spectral Simulation Program, SRI International Report, MP 99-009.
- [7] Wang, G.H. and Clemens, N.T., Effects of imaging system blur on measurements of flow scalars and scalar gradients, *Experiments in Fluids* 37 (2004) 194-2.
- [8] Chen, Y.-C., Peters, N., Schneemann, G.A., Wruck, N., Renz, U. and Mansour M.S., Highly Strained Turbulent Rich Methane Flames Stabilized by Hot Combustion Products *Combust. Flame* 107 (1996) 223-244.
- [9] Wu, M.S., Kwon, S., Driscoll, J.F., Faeth, G. M., Preferential Diffusion Effects on the Surface Structure of Turbulent Premixed Hydrogen/Air Flames, *Combust. Sci. and Tech.* 78 (1991) 69-96.
- [10] Cabra, R., Myhrvold, T., Chen, J.Y., Dibble, R.W., Karpets, A.N. and Barlow, R.S., Simultaneous Laser Raman-Rayleigh-LIF Measurements and Numerical Modeling Results of a Lifted Turbulent H₂/N₂ Jet Flame in a Vitiated Coflow., *Proc. Combust. Inst.* 29 (2002) 1881-1888.